MNRAS 000, 1–7 (2020) Preprint 16 February 2021 Compiled using MNRAS LATEX style file v3.0

Eccentric Dynamical Tides

Yubo Su[1], Dong Lai[1]
[1] *Cornell Center for Astrophysics and Planetary Science, Department of Astronomy, Cornell University, Ithaca, NY 14853, USA*

Accepted XXX. Received YYY; in original form ZZZ

ABSTRACT

Massive stars in eccentric binaries are very important, being the progenitors of neutron star and high-mass X-ray binaries. In such systems, dynamical tides plays a crucial role. However, previous studies of dynamical tides in massive stellar binaries have primarily focused on the case where these binaries are circular. In this work, we revisit the effect of dynamical tides in eccentric, massive stellar binaries and derive analytical expressions that can be used to study binary evolution with arbitrary eccentricities. We apply our results to the radio pulsar J0045–7319, which has a massive B star companion and whose orbital period is rapidly decreasing. In order to reproduce this orbital decay via dynamical tides, we find that the core is likely rotating significantly faster than the measured surface rotation rate. This implies a long core-envelope coupling timescale in B stars.

Key words: keywords

1 INTRODUCTION

Not yet rewritten.

In the course of their evolution, massive stellar binaries give rise to many astrophysical systems of interest including high mass x-ray binaries (HMXRBs) and compact object binaries (CITATION with evolutionary pathway). In general, the more massive star undergoes a supernova before its less massive companion, after which the binary consists of one massive star and one compact object in an eccentric orbit (MS-CO binary). In such a system, the evolution is dominated by the torque from the compact object on the massive star due to dynamical tides. While this tidal torque is now well understood for circular binaries (Kushnir et al. 2017), it has not been carefully studied for binaries with substantial eccentricities. The tidal evolution of such eccentric binaries sculpt the population of HMXRBs (CITE) as well as the population of compact object binaries (Vigna-Gómez et al. 2020).

The dissipation due to the dynamical tide in a massive star's envelope under the influence of a *circular* perturber is traditionally understood via Zahn's parameterized theory of dynamical tides (Zahn 1975). However, Zahn's theory relies on a dimensionless parameter E_2 reflecting the detailed stellar structure that varies over many orders of magnitudes for typical stars. In general, the value of E_2 is taken from empirical fits to simplified stellar models (Hurley et al. 2002; Vigna-Gómez et al. 2020). The introduction of this uncertain parameter E_2 is because the dynamical tidal torque arises due to excitation of internal gravity waves at the radiative convective boundary (RCB) (Goldreich & Nicholson 1989; Savonije & Papaloizou 1983), but Zahn's formula is evaluated at the *stellar* radius. Instead, it is possible re-express the tidal torque in terms of quantities evaluated at the RCB itself, for which dimensionless parameters are generally of order unity for a wide range of stars (Kushnir et al. 2017). However, Kushnir et al. (2017) only consider circular binaries.

To study the dynamical tide in eccentric binaries, it is natural to decompose the perturbing potential into Fourier harmonics, each of which is analogous to a perturber on a circular orbit (e.g. Storch & Lai 2013; Vick et al. 2017). While accurate, such decompositions are unwieldy to evaluate as the eccentricity increases, often requiring summing hundreds of terms and lending little intuition to the broad scalings of the tidal torque. In this work, we show that, for the circular torque given by Kushnir et al. (2017), an accurate, approximate, closed form for the dynamical tide in a highly eccentric MS-CO binary can be obtained. Contrary to existing models of dynamical tides (e.g. Vigna-Gómez et al. 2020), our formulation improves in accuracy as the binary eccentricity increases. We give closed forms for both the tidal torque and inspiral rate of such an MS-CO binary.

In Section 2, we review the relevant equations. In Sections 3.1 and 3.2, we derive accurate, approximate closed forms for the torque and energy transfer rate in the binary. In Section 4, we apply results to the binary radio pulsar J0045-7319. We conclude and discuss in Section 5.

2 TIDAL TORQUE IN MASSIVE STARS

2.1 Circular Orbit

We first review the case where the MS-CO binary is circular. Let M_2 be the mass of the CO, a be the semimajor axis of the binary, and Ω the orbital angular frequency of the binary. The tidal torque exerted on the star by the companion is (Kushnir et al. 2017):

$$T_{\rm circ}(\omega) = T_0\,{\rm sgn}\,(\omega)\left|\frac{\omega}{\Omega}\right|^{8/3}, \tag{1}$$

$$T_0 \equiv \beta_2 \frac{GM_2^2 r_{\rm c}^5}{a^6}\left(\frac{\Omega}{\sqrt{GM_{\rm c}/r_{\rm c}^3}}\right)^{8/3}\frac{\rho_{\rm c}}{\bar\rho_{\rm c}}\left(1-\frac{\rho_{\rm c}}{\bar\rho_{\rm c}}\right)^2, \tag{2}$$

$$\beta_2 \equiv \left[\frac{r_{\rm c}}{g_{\rm c}}\left(\frac{{\rm d}N^2}{{\rm d}\ln r}\right)_{r=r_{\rm c}}\right]^{-1/3}\left[\frac{3}{2}\frac{3^{2/3}\Gamma^2(1/3)}{5\cdot 6^{4/3}}\frac{3}{4\pi}\alpha^2\right]. \tag{3}$$

Here, $\omega \equiv \Omega - 2\Omega_{\rm s}$ is the tidal forcing frequency, $\Omega_{\rm s}$ is the spin of the massive star, N is the Brünt-Vaisala frequency, r is the radial

coordinate within the star, and $r_c, M_c, g_c, \rho_c, \bar{\rho}_c$ are the radius of the RCB, the mass contained within the convective core, the gravitational acceleration at the RCB, the stellar density at the RCB, and the average density of the convective core, respectively. α and β_2 are numerical constants defined by Kushnir et al. (2017), where $\beta_2 \approx 1$ is a good approximation for a large range of stellar models. In Eq. (1), we have written the terms such that T_0 contains all the spin-independent terms.

2.2 Eccentric Orbit

The gravitational potential of an eccentric companion to quadrupolar order can be decomposed as a sum over circular orbits (e.g. Storch & Lai 2013; Vick et al. 2017):

$$U = \sum_{m=-2}^{2} U_{2m}(\vec{r}, t), \tag{4}$$

$$\begin{aligned} U_{2m}(\vec{r}, t) &= -\frac{GM_2 W_{2m} r^2}{D(t)^3} Y_{2m}(\theta, \phi) e^{-imf(t)}, \\ &= -\frac{GM_2 W_{2m} r^2}{a^3} Y_{2m}(\theta, \phi) \sum_{N=-\infty}^{\infty} F_{Nm} e^{-iN\Omega t}. \end{aligned} \tag{5}$$

Here, (r, θ, ϕ) are the radial, polar, and azimuthal coordinates of $\vec{r}$ respectively, $W_{2\pm2} = \sqrt{3\pi/10}$, $W_{2\pm1} = 0$, $W_{20} = -\sqrt{\pi/5}$, $D(t)$ is the instantaneous distance between the star and companion, f is the true anomaly, Y_{lm} denote the spherical harmonics, and Ω is the mean motion of the companion. F_{Nm} denote the *Hansen coefficients* for $l = 2$ (also denoted X^n_{2m} in Murray & Dermott 1999), which are defined implicitly in Eq. (5) to be the Fourier coefficients of the perturbing function, i.e.

$$\frac{a^3}{D(t)^3} e^{-imf(t)} = \sum_{N=-\infty}^{\infty} F_{Nm} e^{-iN\Omega t}. \tag{6}$$

The F_{Nm} can be written explicitly as an integral over the eccentric anomaly (Murray & Dermott 1999; Storch & Lai 2013):

$$F_{Nm} = \frac{1}{\pi} \int_0^{\pi} \frac{\cos\left[N(E - e\sin E) - mf(E)\right]}{(1 - e\cos E)^2} \, \mathrm{d}E. \tag{7}$$

By considering the effect of each summand in Eq. (5), the total torque on the star, energy transfer in the inertial frame, and heating in the star's corotating frame can be obtained (Storch & Lai 2013; Vick et al. 2017):

$$T = \sum_{N=-\infty}^{\infty} F_{N2}^2 T_{\rm circ}(N\Omega - 2\Omega_{\rm s}), \tag{8}$$

$$\begin{aligned} \dot{E}_{\rm in} = \frac{1}{2} \sum_{N=-\infty}^{\infty} \Bigg\{ &\left(\frac{W_{20}}{W_{22}}\right)^2 N\Omega F_{N0}^2 T_{\rm circ}(N\Omega) \\ &+ N\Omega F_{N2}^2 T_{\rm circ}(N\Omega - 2\Omega_{\rm s}) \Bigg\}, \end{aligned} \tag{9}$$

$$\dot{E}_{\rm rot} = \dot{E}_{\rm in} - \Omega_{\rm s} T. \tag{10}$$

Here, dots indicate time derivatives.

From these, we can obtain the binary inspiral and circularization times using:

$$\frac{\dot{a}}{a} = \frac{\dot{E}_{\rm in}}{E_{\rm orb}}, \tag{11}$$

$$\frac{\dot{e}}{e} = \left(\frac{\dot{E}_{\rm in}}{2E_{\rm orb}} + \frac{T}{L_{\rm orb}}\right)\left(\frac{1 - e^2}{e^2}\right). \tag{12}$$

where $E_{\rm orb} = -GMM_2/2a$ is the orbital binding energy and $L_{\rm orb} = \sqrt{G(M + M_2)\, a\,(1 - e^2)}$ is the orbital angular momentum. The stellar synchronization time can also be computed assuming that the star rotates rigidly[1]:

$$\frac{\dot{\Omega}_{\rm s}}{\Omega_{\rm s}} = \frac{T}{kMR^2\Omega_{\rm s}}, \tag{13}$$

where kMR^2 is the angular momentum of the star.

3 ANALYTIC EVALUATION OF TIDAL TORQUE AND ENERGY TRANSFER

The objective of this paper is to study the effect of dynamical tides in an eccentric MS-CO binary. First, we compute the tidal torque by substituting the torque due to a CO on a circular orbit [Eq. (1)] into the summation Eq. (8), obtaining

$$T = \sum_{N=-\infty}^{N=\infty} F_{N2}^2 T_0 \,\mathrm{sgn}\left(N - \frac{2\Omega_{\rm s}}{\Omega}\right)\left|N - \frac{2\Omega_{\rm s}}{\Omega}\right|^{8/3}. \tag{14}$$

The energy transfer rate in the inertial frame is similarly obtained by substituting Eq. (1) into Eq. (9)

$$\begin{aligned} \dot{E}_{\rm in} = \frac{T_0}{2} \sum_{N=-\infty}^{\infty} \Bigg[&N\Omega F_{N2}^2 \mathrm{sgn}\left(N - 2\Omega_{\rm s}/\Omega\right) |N - 2\Omega_{\rm s}/\Omega|^{8/3} \\ &+ \left(\frac{W_{20}}{W_{22}}\right)^2 \Omega F_{N0}^2 |N|^{11/3} \Bigg]. \end{aligned} \tag{15}$$

These two expressions give the spin synchronization timescale of the star as well as the inspiral time of the binary due to dynamical tides. While exact, these expressions are difficult to evaluate for larger eccentricities, where one often must sum hundreds or thousands of terms, each of which has a different F_{Nm}. In the subsequent sections, our objective is to obtain closed-form approximations to Eqs. (14–15).

3.1 Approximating Hansen Coefficients

Although the Hansen coefficients can be evaluated using the integral expression Eq. (7), this requires calculating a separate integral for each N. It is more convenient to use the discrete Fourier Transform of the left hand side of Eq. (6) to calculate arbitrarily many N at once (as pointed out by Correia et al. 2014). We can then derive scalings for the Hansen coefficients in the high-eccentricity limit. Since $F_{(-N)m} = F_{N(-m)}$, we will only study the Hansen coefficient behavior for $m \geq 0$.

3.1.1 $m = 2$ Hansen Coefficient Behavior at High Eccentricity

We first consider the case where $m = 2$. Figure 1 shows the F_{N2} for $e = 0.9$. First, we note that F_{N2} is much larger when $N \geq 0$ than for $N < 0$, so we focus on the behavior for $N \geq 0$. Here, F_{N2} has only one substantial peak. There are two characteristic frequency scales, Ω and $\Omega_{\rm p}$ the pericenter frequency, defined by

$$\Omega_{\rm p} \equiv \Omega \frac{\sqrt{1 + e}}{(1 - e)^{3/2}}. \tag{16}$$

[1] Note that the process of stellar synchronization is not expected to be uniform (Goldreich & Nicholson 1989; Su et al. 2020), as the generated torque depends on the core spin but deposits angular momentum in the envelope.

For convenience, we also define N_p as the floor of Ω_p/Ω, i.e.

$$N_\mathrm{p} \equiv \lfloor \Omega_\mathrm{p}/\Omega \rfloor, \tag{17}$$

Since N_p is the largest harmonic scale, we expect that the peak of the F_{N2} should occur at $\sim N_\mathrm{p}$. When $N \gg N_\mathrm{p}$, the Fourier coefficients must fall off exponentially by the Paley-Wiener theorem since the left hand side of Eq. (6) is smooth. On the other hand, when $N \ll N_\mathrm{p}$, since there are no characteristic frequenciees between Ω and Ω_p, we expect that the Hansen coefficients must be scale free between $N = 1$ and N_p, i.e. a power law. Both of these characteristics are reflected in Fig. 1.

Motivated by these considerations, we assume the Hansen coefficients can be approximated by

$$F_{N2} \approx \begin{cases} C_2 N^p e^{-N/\eta_2} & N \geq 0, \\ 0 & N < 0, \end{cases} \tag{18}$$

for some fitting coefficients C_2, p, and η_2. By performing fits to F_{N2}, we found that $p \approx 2$ is relatively constant for modest-to-large eccentricities[2]. For the remainder of this work, we take $p = 2$ to be fixed.

To constrain the remaining two free parameters η_2 and C_2 the normalization, we use the well known Hansen coefficient moments (Hut 1981)

$$\sum_{N=-\infty}^{\infty} F_{N2}^2 = \frac{f_5}{\left(1-e^2\right)^{9/2}}, \tag{19}$$

$$f_5 \equiv 1 + 3e^2 + \frac{3e^4}{8}, \tag{20}$$

$$\sum_{N=-\infty}^{\infty} F_{N2}^2 N = \frac{2 f_2}{\left(1-e^2\right)^{6}}, \tag{21}$$

$$f_2 \equiv 1 + \frac{15e^2}{2} + \frac{45e^4}{8} + \frac{5e^6}{16}. \tag{22}$$

This fixes

$$\eta_2 = \frac{4 f_2}{5 f_5 \left(1-e^2\right)^{3/2}}, \tag{23}$$

$$C_2 = \left[\frac{4 f_5}{3\left(1-e^2\right)^{9/2} \eta_2^5} \right]^{1/2}. \tag{24}$$

Despite having zero free parameters, this formula accurately describes the F_{N2} as can be seen in Fig. 1.

3.1.2 $m = 0$ *Hansen Coefficient Behavior at High Eccentricity*

We now turn to the $m = 0$ Hansen coefficients, F_{N0}, which are shown in Fig. 2. We know that $F_{N0} = F_{(-N)0}$, so we consider only $N \geq 0$. From the figure, we see that the F_{N0} decay exponentially.

[2] This can be understood, as the left hand side of Eq. (6) resembles the second derivative of a Dirac delta when the eccentricity is substantial: it is sharply peaked about $t = 0$, is periodic with period $P = 2\pi/\Omega$, and has zero derivative three times every period (at $t = \epsilon$, $t = P/2$, and $t = P - \epsilon$ for some small $\epsilon \sim \Omega_\mathrm{p}^{-1}$). This characteristics suggest that it resembles the second derivative of a Gaussian with width $\sim \Omega_\mathrm{p}^{-1}$. For timescales $\gtrsim \Omega_\mathrm{p}^{-1}$, this Gaussian further resembles the Dirac delta function, which has a flat Fourier spectrum ($\propto N^0$). Since time differentiation multiplies by N in frequency space, we see indeed that $F_{N2} \propto N^2$ for $N \lesssim N_\mathrm{p}$.

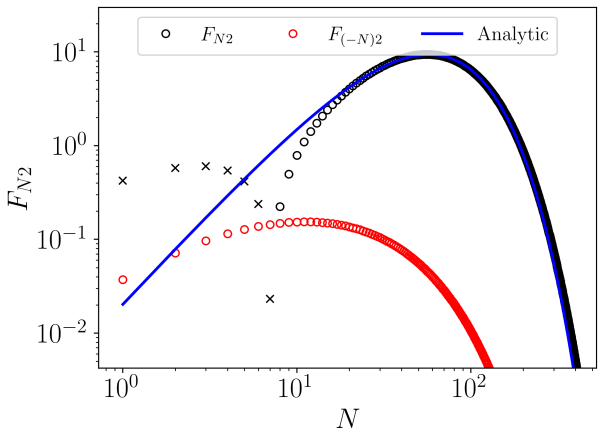

Figure 1. Plot of Hansen coefficients F_{N2} for $e = 0.9$. The red circles denote negative N, while the black circles and crosses denote positive and negative F_{N2}. The blue line is the formula given by Eq. (18) with η_2 and C_2 given by Eqs. (23–24).

By dimensional analysis, this decay must occur over scales $\sim N_\mathrm{p}$. Therefore, we naturally assume the F_{N0} scale as

$$F_{N0} = C_0 e^{-|N|/\eta_0}. \tag{25}$$

The two free parameters C_0 and η_0 are constrained by the well known moments (Hut 1981)

$$\sum_{N=-\infty}^{\infty} F_{N0}^2 = \frac{f_5}{\left(1-e^2\right)^{9/2}}, \tag{26}$$

$$\sum_{N=-\infty}^{\infty} F_{N0}^2 N^2 = \frac{9e^2}{2\left(1-e^2\right)^{15/2}} f_3, \tag{27}$$

$$f_3 = \frac{1}{2} + \frac{15e^2}{8} + \frac{15e^4}{16} + \frac{5e^6}{128}. \tag{28}$$

We have defined the common functions f_3 and f_5. This then requires

$$\eta_0 = \left[\frac{9e^2 f_3}{\left(1-e^2\right)^3 f_5} \right]^{1/2}, \tag{29}$$

$$C_0 = \left[\frac{f_5}{\left(1-e^2\right)^{9/2} \eta_0} \right]^{1/2}. \tag{30}$$

The good agreement of this analytic formula can be seen in Fig. 2.

3.2 Approximate Expressions for Torque and Energy Transfer

Having found good approximations for the Hansen coefficients, we now apply them to simplify the formulas for the torque and the energy transfer rate in Section 3.

3.2.1 *Tidal Torque*

Towards simplifying the torque, given by Eq. (14), we replace F_{N2} with Eq. (18) and the sum with an integral, obtaining

$$T \approx T_0 \int_0^\infty C_2^2 N^4 e^{-2N/\eta_2} \operatorname{sgn}\left(N - 2\Omega_\mathrm{s}/\Omega\right) \left|N - 2\Omega_\mathrm{s}/\Omega\right|^{8/3} \mathrm{d}N. \tag{31}$$

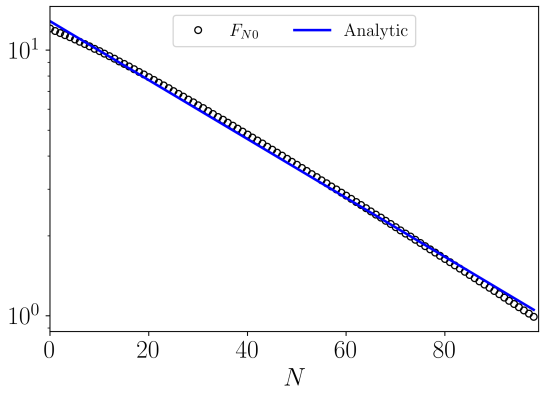

Figure 2. Plot of F_{N0} (black circles) for $e = 0.9$. Since $F_{N0} = F_{(-N)0}$, we only show positive N. The blue line is given by Eq. (25) with η_0 and C_0 given by Eqs. (29–30).

To further simplify this expression, we first analyze it in the zero spin limit. Here, Eq. (31) can be integrated analytically[3], giving

$$\lim_{\Omega_s \to 0} T = T_0 \frac{f_5(\eta_2/2)^{8/3}}{(1-e^2)^{9/2}} \frac{\Gamma(23/3)}{4!}. \tag{32}$$

The accuracy of this formula is shown in the top panel of Fig. 3. For comparison, we also illustrate the torque predicted by direct integration of Eq. (14). It can be see that both the integral and the analytic closed form perform well for moderate-to-large eccentricities, but both overpredict the torque at small e. This suggests that approximating the Hansen coefficient sum with an integral is inaccurate when the eccentricity is small. This is expected, as the number of nonnegligible Hansen coefficients is small when the eccentricity is small, so the continuum approximation is poor.

Eq. (32) is valid so long as $\Omega_s/\Omega \ll \eta_2$, since the integrand is maximized when $N \sim \eta_2$. If instead $\Omega_s/\Omega \gg \eta_2$, Eq. (14) can be evaluated directly with the known Hansen coefficient moments, which gives

$$\lim_{\Omega_s \to \infty} T = -T_0 \,\mathrm{sgn}(\Omega_s)\ |2\Omega_s/\Omega|^{8/3} \frac{f_5}{(1-e^2)^{9/2}}. \tag{33}$$

The accuracy of this formula is shown in the bottom panel of Fig. 3 for $\Omega_s/\Omega = 400$ along with the integral expression. $400 \gg \eta_2$ for the depicted eccentricities. We see that direct summation, the integral expression, and Eq. (33) all agree very well for all eccentricities.

We now have the asymptotic forms of Eq. (31) for small and large spins, but we can derive an approximation valid for all spins. To do this, we first analyze the regime where the spin is small but non-negligible. In this regime, we approximate

$$N - 2\Omega_s/\Omega \simeq \frac{N}{N_{\max}} \left(N_{\max} - \frac{2\gamma_T \Omega_s}{\Omega} \right), \tag{34}$$

for some free parameter γ_T. Using this, we can integrate Eq. (31), and then γ_T is fixed by requiring our expression reproduce the large spin limit [Eq. (33)] when taking $|\Omega_s| \to \infty$. This procedure thus connects the two asymptotic forms Eq. (33–32), and we obtain

$$T = T_0 \frac{f_5(\eta_2/2)^{8/3}}{(1-e^2)^{9/2}}\ \mathrm{sgn}\left(1 - \gamma_T \frac{\Omega_s}{\eta_2 \Omega}\right) \left| \frac{4}{\gamma_T} \left(1 - \gamma_T \frac{\Omega_s}{\eta_2 \Omega}\right) \right|^{8/3}, \tag{35}$$

$$\gamma_T = 4 \left(\frac{4!}{\Gamma(23/3)} \right)^{3/8} \approx 0.691. \tag{36}$$

Fig. 4 demonstrates the accuracy of this prediction as a function of Ω_s. As expected from the construction of this approximation, both the large and small spin limits are well captured, and the scaling for intermediate spins is also rather accurate. It is worth noting that integration of Eq. (31) is markedly more accurate than the closed form when T changes signs. To interpret this, we recall that the integral uses our approximate form for the Hansen coefficients but handles the spin dependence exactly. This suggests that our approximation in handling the spin dependence [Eq. (41)] is the dominant source of error when T is near zero. Again, this is expected, as when $e = 0.9$, Eq. (14) is the sum over many non-negligible Hansen coefficients and thus can be well approximated by an integral. In summary, the tidal torque must be evaluated with explicit summation [Eq. (14)] when e is small, must be evaluated with the integral expression [Eq. (31)] when $\Omega_s \simeq \Omega_p$, and otherwise can be evaluated using the explicit formula given by Eq. (35).

3.2.2 *Pseudosynchronization*

The torque, given by Eq. (35), vanishes for a single Ω_s. We call this spin the pseudosynchronization spin frequency, given by

$$\frac{\Omega_{ps}}{\Omega} = \frac{\eta_2}{\gamma_T} = \frac{4 f_2}{5 \gamma_T f_5 \left(1-e^2\right)^{3/2}}. \tag{37}$$

This has the expected scaling $\Omega_{ps} \simeq \Omega_p$. By comparison, in standard weak friction theory of equilibrium tides, the pseudo-synchronized rotation rate is given by (Alexander 1973; Hut 1981)

$$\frac{\Omega_{ps}^{(Eq)}}{\Omega} = \frac{f_2}{f_5 \left(1-e^2\right)^{3/2}}. \tag{38}$$

This differs from our Eq. (37) by a factor of 1.15. Figure 5 compares these two predictions, as well as Ω_p, to applying a root finding algorithm to Eq. (8). Ω_p is very nearly equal to $\Omega_{s,ps}$, and both are slightly better estimates for the pseudosynchonization spin frequency than $\Omega_{ps}^{(Eq)}$.

Note that, very near the pseudosynchronized spin frequency, Eq. (35) predicts that $\mathrm{d}T/\mathrm{d}\Omega_s \approx 0$. This is not physically accurate and is an artifact of our factorization ansatz in Eq. (41).

3.2.3 *Energy Transfer*

We now turn our attention to Eq. (9) and replace F_{N2} and F_{N0} with their approximations [Eqs. (18) and (25)] to obtain

$$\dot{E}_{in} = \frac{T_0 \Omega}{2} \int_0^\infty \left[C_2^2 N^5 e^{-2N/\eta_2} \mathrm{sgn}\left(N - 2\Omega_s/\Omega\right) |N - 2\Omega_s/\Omega|^{8/3} + 2 \left(\frac{W_{20}}{W_{22}}\right)^2 C_0^2 e^{-2N/\eta_0} N^{11/3} \right] \mathrm{d}N. \tag{39}$$

We evaluate the $m = 2$ and $m = 0$ contributions to this expression separately.

We first examine the $m = 2$ contribution using the same procedure

[3] The key to the success of our approach is that sums of form $\sum_{n=-\infty}^{\infty} F_{N2}^2 N^p$ can be approximated for non-integer p in terms of Γ, since $\int_0^\infty x^p e^{-x}\,\mathrm{d}x = \Gamma(p-1)$. This is not possible with existing analytical techniques.

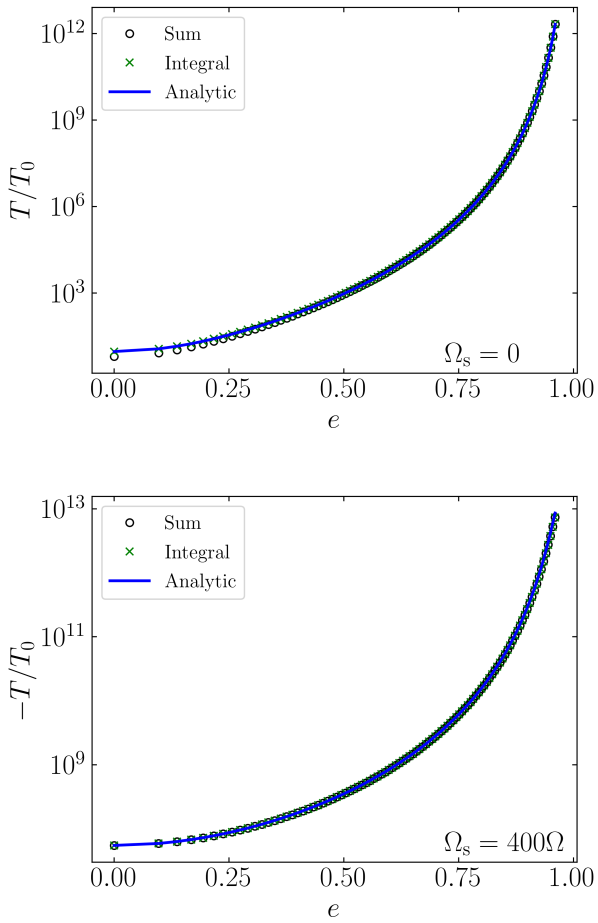

Figure 3. Tidal torque on a non-rotating (top) and rapidly rotating (bottom) star due to a companion with orbital eccentricity e. Black circles represent explicit summation of Eq. (14), green crosses are evaluated using the integral approximation Eq. (31), and the blue line is Eq. (35). In the small and large spin limits, Eq. (35) reduces to Eq. (32) and Eq. (33) respectively.

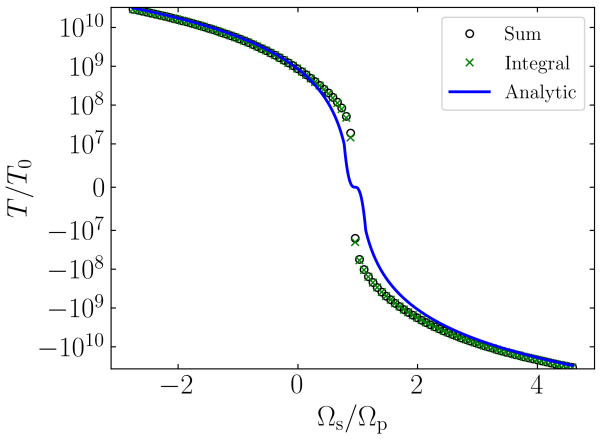

Figure 4. Tidal torque as a function of spin for a highly eccentric $e = 0.9$ companion. Black circles represent direct summation of Hansen coefficients [Eq. (14)], green crosses the integral approximation [Eq. (31)], and solid lines represent the analytic closed form [Eq. (35)]. The spin is normalized by $\Omega_p \approx 43\Omega$ [Eq. (16)].

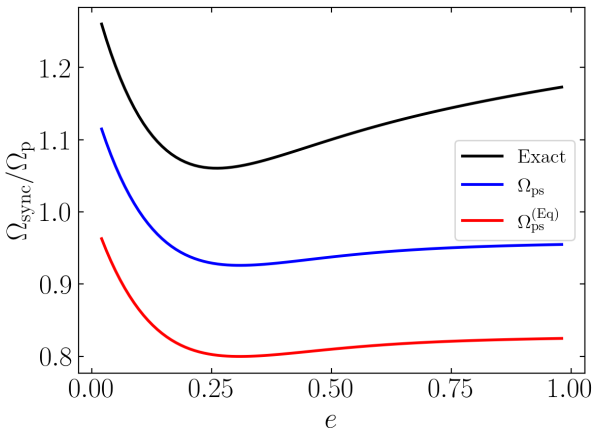

Figure 5. Calculations of the pseudosynchronization spin frequencies Ω_{sync} normalized by the pericenter frequency Ω_p [Eq. (16)] as a function of eccentricity. The blue and red lines are given by Eqs. (37) and (38) respectively. The exact solution, given in the black line, is obtained using finding a root finding algorithm to solve for the zero of Eq. (8).

that was used in Section 3.2.1 for the torque. If the spin is large, $\Omega_s/\Omega \gg \eta_2$, the $m = 2$ contribution evaluates to

$$\lim_{\Omega_s \to \infty} \dot{E}_{in}^{(m=2)} = -\frac{T_0 \Omega}{2} \, \mathrm{sgn}(\Omega_s) |2\Omega_s/\Omega|^{8/3} \frac{2 f_2}{(1-e^2)^6}. \tag{40}$$

If the spin is instead moderate, $\Omega_s/\Omega \lesssim \eta/2$, we make the approximation

$$N - 2\Omega_s/\Omega \simeq \frac{N}{N_{max}} \left(N_{max} - \frac{2\gamma_E \Omega_s}{\Omega} \right), \tag{41}$$

where γ_E is a free parameter. This lets us integrate the $m = 2$ component of Eq. (39) analytically, and we can constrain γ_E by requiring the integral agree with Eq. (40). This yields

$$\dot{E}_{in}^{(m=2)} = \frac{T_0 \Omega f_5 (\eta_2/2)^{11/3}}{2(1-e^2)^{9/2}} \times \mathrm{sgn}\left(1 - \gamma_E \frac{\Omega_s}{\eta_2 \Omega}\right) \left| \frac{4}{\gamma_E} \left(1 - \gamma_E \frac{\Omega_s}{\eta_2 \Omega}\right) \right|^{8/3}, \tag{42}$$

$$\gamma_E = 4 \left(\frac{5!}{\Gamma(26/3)} \right)^{3/8} \approx 0.5886. \tag{43}$$

The $m = 0$ contribution to Eq. (39) is much more straightforward and can be directly integrated using the parameterization Eq. (25). So we obtain the total energy transfer rate

$$\dot{E}_{in} = \frac{T_0 \Omega}{2} \left[\frac{f_5 (\eta_2/2)^{11/3}}{(1-e^2)^{9/2}} \frac{\Gamma(26/3)}{4!} \times \mathrm{sgn}\left(1 - \gamma_E \frac{\Omega_s}{\eta_2 \Omega}\right) \left| 1 - \gamma_E \frac{\Omega_s}{\eta_2 \Omega} \right|^{8/3} + \frac{f_5 \Gamma(14/3)}{(1-e^2)^{10}} \left(\frac{3}{2}\right)^{8/3} \left(\frac{e^2 f_3}{f_5}\right)^{11/6} \right]. \tag{44}$$

In Fig. 6, we show the agreement of Eq. (44) in the small and

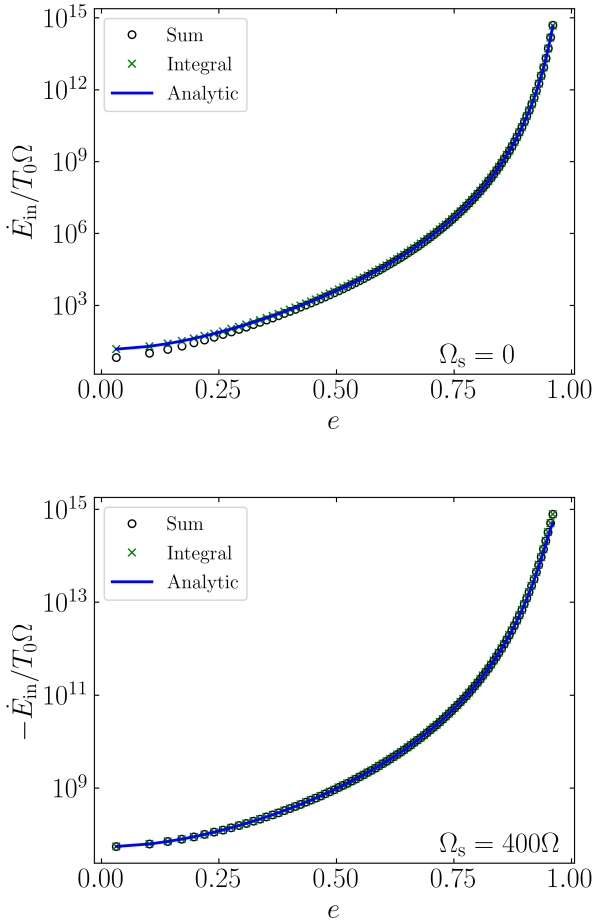

Figure 6. Plot of $\dot{E}_{in}$ for a non-rotating (top) and a rapidly rotating (bottom) star. Black circles represent explicit summation of the Hansen coefficients as in Eq. (**??**), green crosses the integral form Eq. (39), and the blue line the closed form Eq. (44).

large spin limits, where good agreement is observed both with the integral form Eq. (39) and the closed form Eq. (44). Again, when the spin and eccentricity are both negligible, both the integral and closed form expressions overpredict the energy dissipation rate. In Fig. 7, we show the energy transfer rate using both the integral and analytic closed forms as a function of spin when $e = 0.9$. The performance of the analytic expression degrades near pseudosynchronization but generally captures the correct scaling, while the integral expression remains accurate for all spins.

4 EXAMPLE SYSTEM: PSR J0045+7319

As an example of our calculations above, we consider PSR J0045-7319 binary system (Bell et al. 1995). The system was initially reported to have pulsar mass $M_2 = 1.4M_\odot$, $q = 6.3$, $e = 0.808$, orbital period $P = 51.17$ days, and $\dot{P} = -3.03 \times 10^{-7}$ (Kaspi et al. 1996). This gives a mass of $M = 8.8M_\odot$ for the massive star and an orbital separation $a = 126R_\odot$. Furthermore, the measured luminosity $L = 1.2 \times 10^4 L_\odot$ and surface temperature $T_{surf} = (24000 \pm 1000)$ K give the radius of the star to be $R = 6.4R_\odot$ (Kaspi et al. 1996). The internal structure of the star can be obtained by comparison

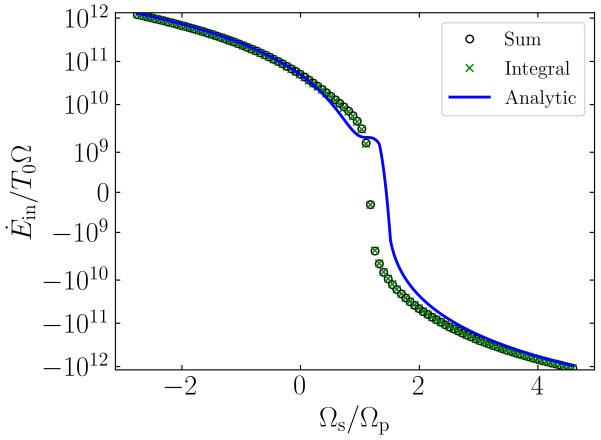

Figure 7. $\dot{E}_{in}$ as a function of spin [normalized by Ω_p; Eq. (16)] for a highly eccentric $e = 0.9$ companion. Black circles represent direct summation of Hansen coefficients, green crosses the integral approximation, and the blue line the analytic closed form.

to detailed stellar structure calculations, yielding $M_c \approx 3M_\odot$ and $r_c \approx 1.38R_\odot$ (Kumar & Quataert 1998). To account for uncertainties in the stellar structure, we take this M_c to be fixed and consider a range of $r_c \in [0.7, 1.5]$. To compute the tidal torque, we must also make assumptions about the ratio $\rho_c/\bar{\rho}_c$, which can only be obtained via stellar structure simulations. We take $\rho_c/\bar{\rho}_c \approx 1/3$ as a fiducial value (though in reality this likely varies with r_c).

Figure 8 shows $\dot{P}$ as a function of Ω_s, using Eq. (44), evaluated using four different r_c. The measured $\dot{P}$ is shown by the horizontal dashed line. Note that for the most compact core radius $r_c = 0.7R_\odot$, there are no solutions for Ω_s; even a maximally spinning core cannot generate enough tidal dissipation to match the observed $\dot{P}$. Substantial retrograde rotation is required to match the predictions, a few times faster than the critical rotation rate of the entire star. As such, strong differential rotation is required between the core and envelope of the star.

5 CONCLUSION AND DISCUSSION

This section is not complete.

The primary results of the paper are approximate expressions for the torque, Eq. (35), and the energy dissipation rate, Eq. (44), in closed form.

- Thanks to some references (Barker & Ogilvie, my work), there seems to be some evidence that hydrodynamic wave breaking could cause all IGW to break and not reflect, once the pericenter wave reaches nonlinear amplitudes.
- As noted in the text, the approximate forms enforce $dT/d\Omega_s = 0$, which the actual torque does not satisfy. This introduces some slight errors in the exact value of the torque very near pseudosynchronization.
- It is pointed out that the $v \sin i$ for J0045-7319 is 110 ± 10 km/s, while the breakup frequency is $\sqrt{GM/R} = 512$ km/s. Thus, it is expected that the stellar surface is rotating at an appreciable fraction of breakup.
- Obliquity of the star? Dissipation rate should be somewhere between prograde and retrograde.

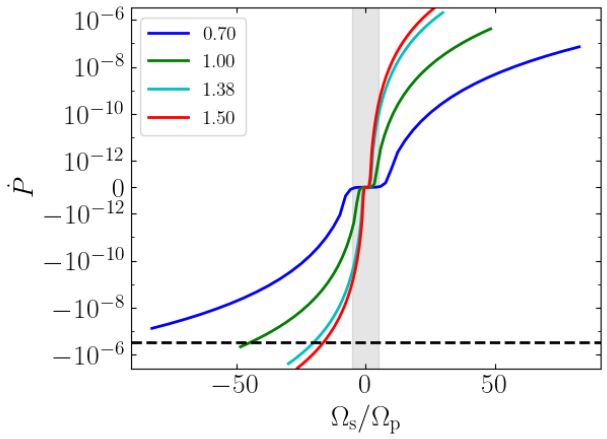

Figure 8. $\dot{P}$ as a function of Ω_s for the canonical parameters for J0045-7319, as evaluated by explicit summation of Eq. (15), for four different values of r_c (legend, in units of $R_\odot$). The measured $\dot{P} = -3.03 \times 10^{-7}$ is shown by the horizontal dashed line. The vertical shaded region is the region where Ω_s is less than the breakup rotation rate of the star as a whole, given by $\sqrt{GM/R^3}$. Each r_c is only shown for $|\Omega_s| \leq \Omega_{s,c} \equiv \sqrt{GM_c/r_c^3}$ the *core* breakup rotation rate.

- Maybe core is much bigger due to similar process as chemically homogeneous stars?

6 ACKNOWLEDGEMENTS

We thank Michelle Vick, Christopher O'Connor, and Matteo Cantiello for fruitful discussions. YS is supported by the NASA FINESST grant 19-ASTRO19-0041.

REFERENCES

Alexander M., 1973, Astrophysics and Space Science, 23, 459
Bell J., Bessell M., Stappers B., Bailes M., Kaspi V., 1995, The Astrophysical Journal Letters, 447, L117
Correia A. C., Boué G., Laskar J., Rodríguez A., 2014, Astronomy & Astrophysics, 571, A50
Goldreich P., Nicholson P. D., 1989, Astrophysical Journal, 342, 1079
Hurley J. R., Tout C. A., Pols O. R., 2002, Monthly Notices of the Royal Astronomical Society, 329, 897
Hut P., 1981, Astronomy and Astrophysics, 99, 126
Kaspi V., Bailes M., Manchester R., Stappers B., Bell J., 1996, Nature, 381, 584
Kumar P., Quataert E. J., 1998, The Astrophysical Journal, 493, 412
Kushnir D., Zaldarriaga M., Kollmeier J. A., Waldman R., 2017, Monthly Notices of the Royal Astronomical Society, 467, 2146
Murray C. D., Dermott S. F., 1999, Solar system dynamics. Cambridge university press
Savonije G., Papaloizou J., 1983, Monthly Notices of the Royal Astronomical Society, 203, 581
Storch N. I., Lai D., 2013, Monthly Notices of the Royal Astronomical Society, 438, 1526
Su Y., Lecoanet D., Lai D., 2020, Monthly Notices of the Royal Astronomical Society, 495, 1239
Vick M., Lai D., Fuller J., 2017, Monthly Notices of the Royal Astronomical Society, 468, 2296
Vigna-Gómez A., MacLeod M., Neijssel C. J., Broekgaarden F. S., Justham S., Howitt G., de Mink S. E., Mandel I., 2020, arXiv preprint arXiv:2001.09829
Zahn J.-P., 1975, Astronomy and Astrophysics, 41, 329

This paper has been typeset from a TEX/LATEX file prepared by the author.